

Effect of Ag on Sn–Cu and Sn–Zn lead free solders

S.N. ALAM*, PRERNA MISHRA, RAJNISH KUMAR

Department of Metallurgical and Materials Engineering, National Institute of Technology Rourkela, Orissa, Pin-769008, India

Lead and lead-containing compounds are considered as toxic substances due to their detrimental effect on the environment. Sn-based soldering systems, like Sn–Cu and Sn–Zn are considered as the most promising candidates to replace the eutectic Sn–Pb solder compared to other solders because of their low melting temperature and favorable properties. Eutectic Sn–0.7 wt.% Cu and near eutectic composition Sn–8 wt.% Zn solders have been considered here for study. For the Sn–Cu system, besides the eutectic Sn–0.7 wt.% Cu composition, Sn–1Cu and Sn–2Cu were studied. Three compositions containing Ag: Sn–2Ag–0.7Cu, Sn–2.5Ag–0.7Cu and Sn–4.5Ag–0.7Cu were also developed. Ag was added to the eutectic Sn–0.7 wt.% Cu composition in order to reduce the melting temperature of the eutectic alloy and to enhance the mechanical properties. For the Sn–Zn system, besides the Sn–8 wt.% Zn near eutectic composition, Sn–8Zn–0.05Ag, Sn–8Zn–0.1Ag and Sn–8Zn–0.2Ag solder alloys were developed. The structure and morphology of the solder alloys were analyzed using a scanning electron microscope (SEM), field emission scanning electron microscope (FESEM), electron diffraction X-ray spectroscopy (EDX) and X-ray diffraction (XRD). Thermal analysis of the alloys was also done using a differential scanning calorimeter (DSC). Trace additions of Ag have been found to significantly reduce the melting temperature of the Sn–0.7 wt.% Cu and Sn–8 wt.% Zn alloys.

Keywords: Sn–Cu; Sn–Zn; Sn–Cu–Ag; Sn–Zn–Ag; eutectic alloys; thermal analysis

© Wrocław University of Technology.

1. Introduction

An eutectic Sn–Pb solder has been the most widely used material for interconnecting and packaging electronic components. Pb is a major constituent of solder alloys and traditional Sn–Pb solders have been considered as the most popular materials for electronic packaging and assemblies because they have a low melting point, low material cost, good wettability and are easily available. Despite all these advantages a rapid rise in research for finding a suitable lead free solder has occurred due to the inherent toxicity of Pb, which has proven to be a hazard to environment and human health. As a result, attention has been focused on the potential of lead free solders which can provide improved mechanical strength as well as reliability. Elements that can be used in lead free soldering are Cu, Ag, Zn, Bi, Sb, Ni, In, Ge, Al and Cr in a combination with Sn, by making a binary, ternary or quaternary system. Both Sn–Cu and Sn–Zn alloys are

considered as potential candidates for lead free solders [1–5].

Lead free solder alloys are typically Sn-based alloys. Sn is non-toxic and has good corrosion resistance and solderability. This is why using an alloy of Sn with some other low melting point elements could lead to a desirable solder. Sn–Zn solder has low cost and good mechanical properties that are suitable for soldering. Soldering alloys based on the Sn–Cu and Sn–Zn alloy systems have been found to be amongst the most favorable lead free alternatives. The eutectic Sn–0.7Cu alloy is one of the Sn based lead free solder alloys, with small amounts of Cu–Sn intermetallic compound Cu_6Sn_5 precipitated in the Sn matrix. The eutectic Sn–0.7Cu alloy having a melting temperature of 227 °C is one of the most preferred candidates for the lead-free solder for use in electronics interconnections due to its relatively low melting temperature, relatively good solderability and superior mechanical properties compared to other lead free solders. The presence of Cu in Sn-based alloys leads to an improvement in resistance to thermal cycle

*E-mail: nasimulalam@yahoo.com

fatigue and wetting properties due to the formation of intermetallic compounds, like Cu_3Sn and Cu_6Sn_5 . Addition of Ag to the Sn–0.7Cu eutectic solder alloy could reduce the melting point of the eutectic alloy. Apart from this it also helps in decreasing the rate of dissolution of Cu from the Cu substrate. It should be noted that addition of Ag to the Sn–Cu solder raises the cost of the solder to almost 3 times that of the Sn–Pb solder and without adding Ag the cost of the Sn–Cu solder is almost 1.5 times of the Sn–Pb solder. This is the main drawback of the Sn–Ag–Cu solder alloys.

The search for a suitable non-toxic lead free solder alloy with an equivalent melting point close to the eutectic temperature of 183 °C of Sn–37Pb eutectic alloy has posed a considerable challenge. The binary Sn–8.8Zn eutectic lead free solder alloy with a melting temperature of 198 °C is an excellent alternative to the Sn–37Pb solder alloy. It also has very good mechanical properties. Sn–Zn based solder alloy has been found to be a promising candidate and one of the best alternatives to replace the existing Sn–Pb eutectic solder both because of its low cost and melting temperature which is near to Sn–Pb eutectic solder. The low melting temperature of the Sn–Zn eutectic (198 °C) is very close to the Sn–Pb eutectic alloy (183 °C).

Alloying strongly affects the melting temperature, and experimental results indicate that the addition of a small amount of Ag could successfully reduce the melting point of both eutectic Sn–0.7Cu and near eutectic Sn–8Zn solder alloys and also improve the mechanical properties of the alloys. This study examines the effect of Ag addition on the melting point and microstructure of eutectic Sn–0.7Cu and near eutectic Sn–8Zn lead free solders. The present work is devoted to investigate the effects of Ag addition on the microstructure, melting behavior, pasty range, hardness and fracture surface of the Sn–0.7Cu and Sn–8Zn solder alloys [6–11].

2. Experimental

Sn granules were procured from Merck. Cu and Zn were procured from Rankem, RFCL Limited. Ag was procured from Loba Chemie. The

various alloy compositions of the Sn–Cu, Sn–Zn, Sn–Ag–Cu and Sn–Zn–Ag systems were prepared from the granulated Sn, Zn, Cu and Ag powder having purity of 99 %. The elements were mixed in the right proportion and melted in a crucible in a tubular furnace in an inert atmosphere and subsequently cooled in the furnace to produce the solder alloys. The metal was melted in a silica crucible in a muffle furnace. The molten metal was homogenized and furnace cooled. The different Sn–Cu alloy compositions that were selected were Sn–0.7Cu (eutectic), Sn–1Cu and Sn–2Cu alloys. The modification of the eutectic microstructure by trace element addition of Ag into the eutectic alloy system was investigated. For this purpose, Sn–Ag–Cu alloys, like Sn–2Ag–0.7Cu, Sn–2.5Ag–0.7Cu and Sn–4.5Ag–0.7Cu, were developed. Ag was added only to the eutectic Sn–0.7Cu composition to find the effect of addition of Ag. Similarly, for the Sn–Zn system, besides the Sn–8Zn near eutectic composition, Sn–8Zn–0.05Ag, Sn–8Zn–0.1Ag and Sn–8Zn–0.2Ag solder alloys were developed. The furnace was heated to the desired temperature by electrical resistance heating elements. The casting temperature of Sn–Cu, Sn–Zn and Sn–Ag–Cu and Sn–Zn–Ag solder alloys was in the range of 500 to 700 °C. The molten alloys were held at this temperature for 2 h. All the samples were furnace cooled. A scanning electron microscope (SEM) with energy dispersive X-ray spectroscopy (EDX) was used for the microstructural characterization of the solder alloys. The morphology and elemental composition of the samples were analyzed using a JEOL JSM-6480LV scanning electron microscope (SEM) equipped with an INCAP-entaFET-x3 X-ray microanalysis system with a high-angle ultra-thin window detector and a 30 mm² Si(Li) crystal for EDX (energy dispersive X-ray spectroscopy) analysis. A Nova NanoSEM 450/FEI field emission scanning electron microscope (FESEM) was also used for the microstructural characterization of the alloys. Differential scanning calorimetry (DSC) was done in order to determine the melting point of the alloys. The thermal analysis of the samples was done in a Netzsch STA 409C Simultaneous

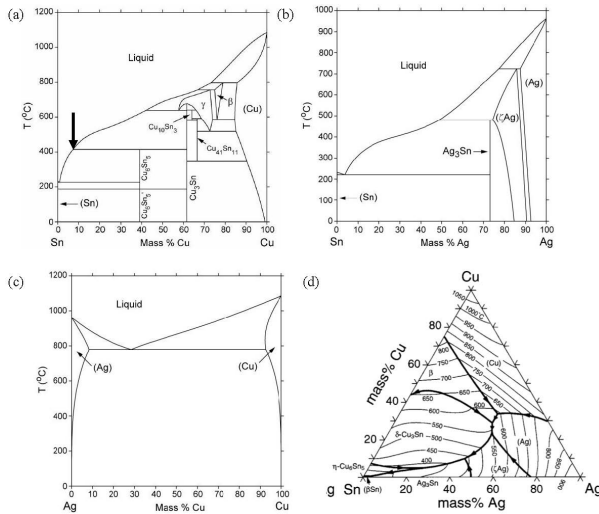


Fig. 1. (a) Sn–Cu (the arrow points the eutectic composition Sn–0.7 wt.% Cu and eutectic temperature 227 °C), (b) Sn–Ag, (c) Ag–Cu binary phase diagrams, (d) Sn–Cu–Ag ternary phase diagram [13].

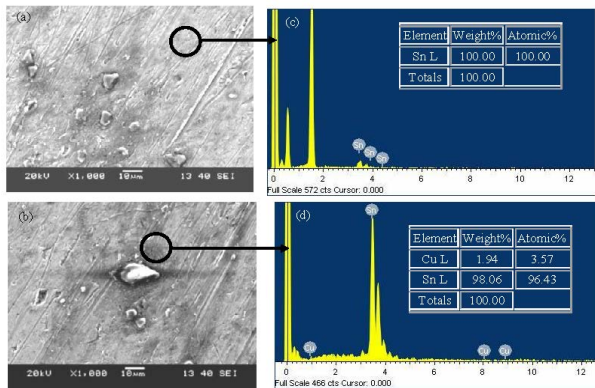


Fig. 2. (a), (b) SEM and (c), (d) EDX analysis of Sn–0.7Cu alloy.

Thermal Analyzer at a heating rate of 10 °C/min in an argon atmosphere in order to determine the melting point of the alloys. X-ray diffraction (XRD) of the alloys was done in a Panalytical PW 3040 X'Pert MPD using Cu K α radiation ($\lambda = 1.54056 \text{ \AA}$) to find out if any new phase was formed during their development. Hardness of the samples was measured using a digital Leco Vickers microhardness tester (LV 700).

3. Results and discussion

The phase diagram of the Sn–Cu system is shown in Fig. 1a. The phase diagram of the Sn–Cu system shows an eutectic reaction at the composition Sn–0.7 wt.% Cu and at a temperature of 227 °C. This eutectic reaction takes place between the intermetallic compound Cu₆Sn₅ and Sn. From the phase diagram of Ag–Sn in Fig. 1b it is clear that the solid solubility of Ag in Sn is very small. The solid solubility of Ag in Sn at the eutectic temperature is only 0.09 at.%. The phases in the Ag–Sn system are the liquid (L), the Ag-rich FCC (Ag) solid solution with a maximum of 11.5 wt.% Sn, the close packed hexagonal ξ (Ag) phase, the orthorhombic short range ordered Ag₃Sn phase (ϵ), the Sn-rich BCT structure (β -Sn) having very low solid solubility of Ag and α -Sn below 13 °C. The equilibrium phases in the Ag–Cu system (Fig. 1c) are liquid (L) with no miscibility gaps, the Ag rich FCC phase, where the maximum solid solubility of Cu in Ag is 14.1 at.% Cu and the Cu-rich FCC phase, where the maximum solid solubility of Ag in Cu is 4.9 at.%. The eutectic temperature of the Ag–Cu system ranges from 777 to 780 °C and the eutectic composition contains 28.1 wt.% Cu. The ternary phase diagram of the Sn–Ag–Cu system in Fig. 1d shows that there are a number of intermetallic compounds, like Cu₆Sn₅, Ag₃Sn and Cu₃Sn in this system. The Sn–Ag–Cu system has a ternary eutectic reaction at 216 °C, $L \rightarrow \eta + \theta + \beta$ -Sn, where $\eta = \text{Cu}_6\text{Sn}_5$ and $\theta = \text{Ag}_3\text{Sn}$.

The eutectic Sn–0.7Cu alloy is one of the Sn-based lead free solder alloys having small amounts of Cu–Sn intermetallic compound precipitated in the Sn matrix. The microstructure of the as-solidified eutectic Sn–0.7Cu solder is shown in Fig. 2a and 2b. The microstructure, as predicted from the phase diagram, consists of β -Sn and the Cu–Sn intermetallic compound Cu₆Sn₅. From the Sn–Cu binary-phase diagram, the volume fraction of Cu₆Sn₅ in the eutectic Sn–Cu alloy can be found using the lever rule and considering the densities of Cu₆Sn₅ (8.28 g/cm³) and Sn (7.31 g/cm³). The volume fraction of Cu₆Sn₅ is found to be only 1.6 %. This is consistent with the SEM

image as only a very small amount of dark colored Cu_6Sn_5 is seen in the SEM images in Fig. 2a and 2b. The light colored regions contain 100 % Sn and no Cu [11–17].

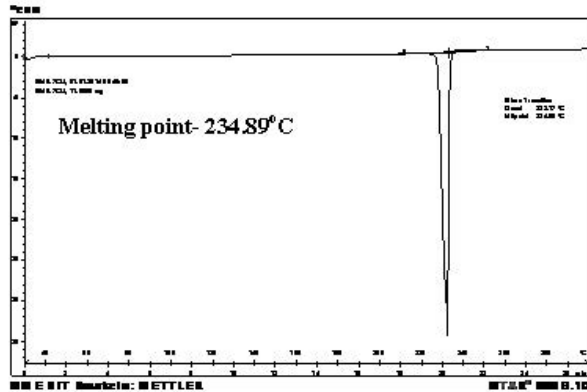


Fig. 3. DSC of Sn–0.7Cu solder alloy.

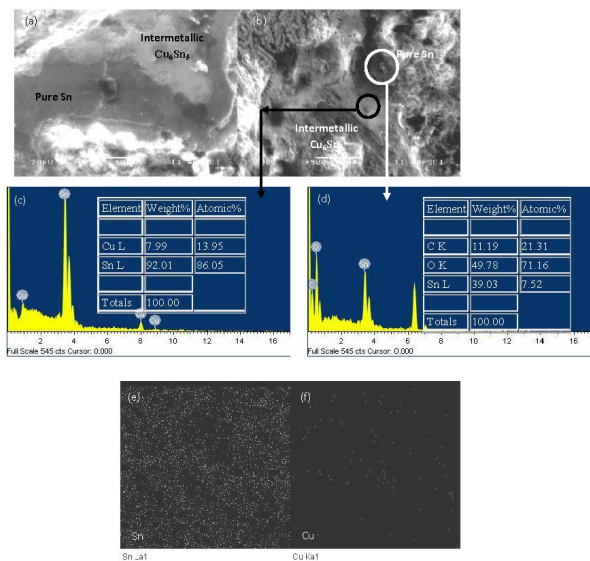


Fig. 4. (a), (b) SEM images of Sn–1 wt.% Cu alloy, (c), (d) EDX analysis of various regions in Sn–1 wt.% Cu alloy and elemental maps of (e) Sn and (f) Cu in the region shown in the SEM image in Fig. 4b.

The DSC analysis in Fig. 3 shows that the melting point of the Sn–0.7Cu solder alloy is 234.89 °C. The eutectic Sn–0.7Cu alloy is known to have a melting temperature of 227 °C. The slight rise in the melting point is possibly due to the presence

of impurities or oxidation of the sample during melting [7].

The microstructure of the near eutectic composition of Sn–1 wt.% Cu solder alloy is shown in Fig. 4a and 4b along with the EDX analysis in Fig. 4c and 4d. The SEM images reveal that there are highly dense regions containing both Cu (7.99 wt.%) and Sn (92.01 wt.%). The grey region containing both Sn and Cu represents the formation of intermetallic compound, possibly Cu_6Sn_5 . The intermetallic Cu_6Sn_5 is highly non-stoichiometric. Cu_6Sn_5 is a well-known intermetallic compound and has an orthorhombic crystal structure. This alloy was prepared at 700 °C in an inert atmosphere. At 700 °C Sn is completely molten (melting point = 231.9 °C). Cu atoms diffuse into Sn, resulting in the formation of the intermetallic Cu_6Sn_5 . On the other hand, the dark regions contain mainly β -Sn and show the absence of Cu in it. The elemental maps of Sn and Cu in Fig. 4e and Fig. 4f, respectively, show that Sn is present almost all over the sample, whereas Cu, which is only in the amount of 1 wt.% in the alloy, is present, where the intermetallic Cu_6Sn_5 is present. Elemental maps have been taken from the region shown in Fig. 4b.

Referring to Fig. 4a and 4b, it can be seen that the Cu_6Sn_5 regions are dispersed in the matrix of β -Sn. The SEM images clearly show the two phase regions of pure Sn and intermetallic Cu_6Sn_5 in the microstructure of Sn–1 wt.% Cu solder alloy. The regions containing dispersed Cu_6Sn_5 are separated by dendritic regions of β -Sn matrix, giving the microstructure a network-like appearance. The DSC result in Fig. 5 shows that the melting point of the near eutectic composition Sn–1 wt.% Cu is 236.82 °C. The rise in the melting point of the near eutectic composition Sn–1 wt.% Cu (236.82 °C) compared to the eutectic Sn–0.7 wt.% Cu solder alloy (234.89 °C) may be due to the presence of higher wt.% of Cu.

Wettability defines the extent to which a liquid can spread on a solid surface. The present aim of our study also focuses on the wetting properties of the Sn–1 wt.% Cu alloy. It can be easily seen from the SEM images in Fig. 6a – 6c that the near eutectic Sn–1 wt.% Cu alloy has good wettability

of the Cu substrate. The EDX analysis in Fig. 6d shows that the region close to the interface between the solder and the Cu substrate contains both Cu (18.35 wt.%) and Sn (37.36 wt.%), indicating the formation of intermetallic Cu_6Sn_5 . There is also a very high percentage of oxygen at the interface. This is possibly due to the oxidation of Cu at the soldering temperature. The region away from the interface contains mainly Sn (93.96 wt.%) and a very low amount of Cu (1.75 wt.%) as seen in the EDX analysis in Fig. 6e.

The SEM image in Fig. 7a shows the microstructure of Sn–2 wt.% Cu solder alloy. This solder alloy is composed of large Sn-rich grains with a fine dispersion of Cu_6Sn_5 intermetallics. The microstructure of the Sn–2Cu solder alloy reveals that the dark colored intermetallic compound Cu_6Sn_5 is finely dispersed in the matrix of β -Sn.

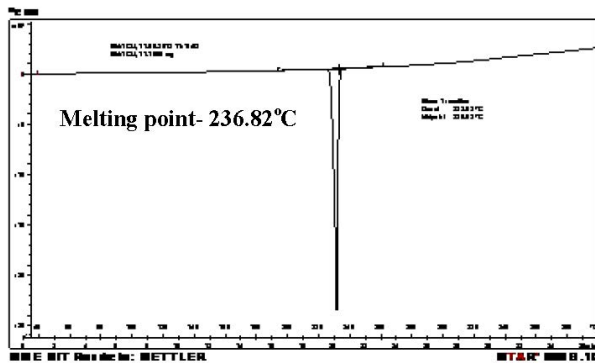


Fig. 5. DSC of Sn–1 wt.% Cu solder alloy.

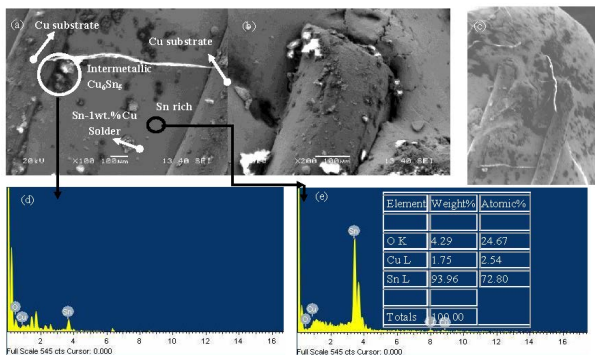


Fig. 6. (a), (b), (c) SEM of Sn–1 wt.% Cu solder on Cu substrate; (d), (e) EDX analysis of the different regions in the solder joint.

EDX analysis in Fig. 7b and 7c reveals the composition of different phases present in the solder alloy. Fig. 7b shows the composition of the dark region in the sample and Fig. 7c presents the composition of the grey region. The grey colored region contains 100 % Sn, whereas the dark region contains both Sn (57.57 wt.%) and Cu (0.26 wt.%). The SEM image in Fig. 7d also suggests that there are two distinct phases in the microstructure of the Sn–2Cu solder alloy. The light colored phase contains almost 100 % Sn and the dark colored phase consists of Sn (36.84 wt.%) and Cu (1.11 wt.%), suggesting the formation of intermetallic compound Cu_6Sn_5 . The elemental mapping of Sn and Cu are shown in Fig. 7e and 7f, respectively. The elemental mapping of the elements have been taken in the region shown in Fig. 7a. The small amount of Cu which forms intermetallic Cu_6Sn_5 seems to be homogeneously distributed in the Sn matrix. The DSC analysis in Fig. 8 shows that the melting point of Sn–2Cu alloy is around 237.88 °C.

Fig. 9a shows the SEM of the solder alloy Sn–2Ag–0.7Cu. This sample shows light colored regions which contain 100 % Sn (Fig. 9b). The dark colored regions are surrounded by light

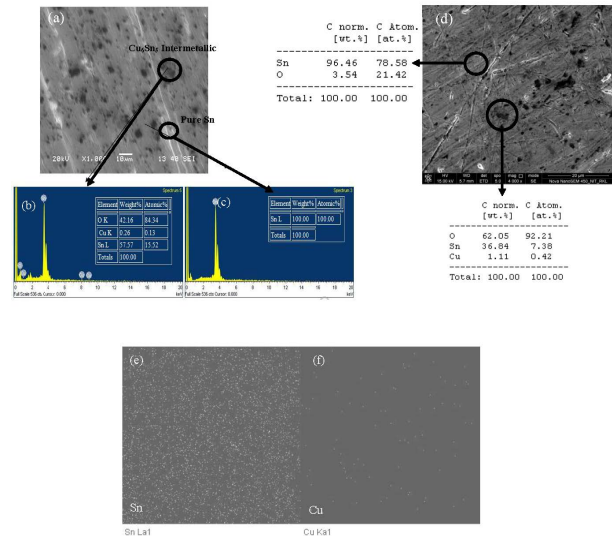


Fig. 7. (a) SEM; (b), (c) EDX analysis of Sn–2Cu solder alloy; (d) SEM image of different areas of the Sn–2Cu solder alloy with EDX analysis. Elemental mapping of (e) Sn, (f) Cu of the region shown in the SEM image in Fig. 7a.

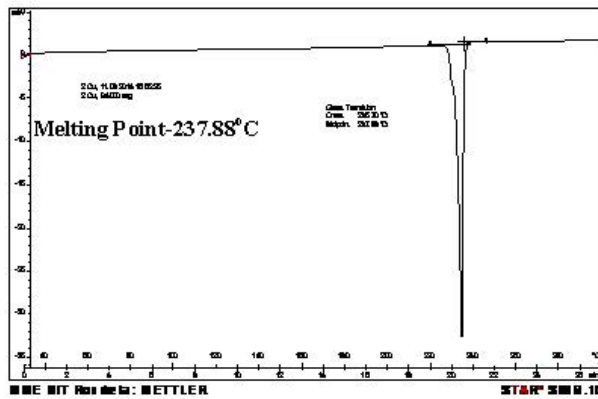


Fig. 8. DSC of Sn–2Cu solder alloy.

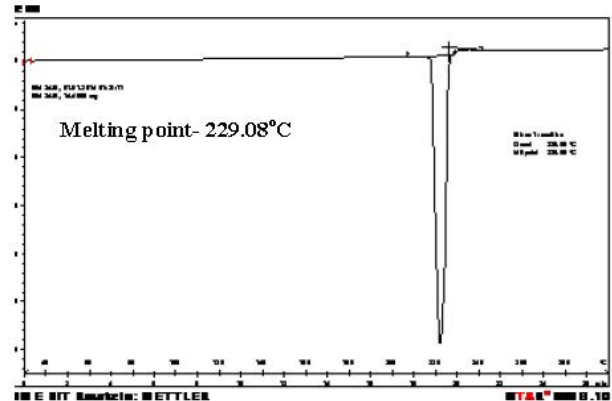


Fig. 10. DSC of Sn–2Ag–0.7Cu solder alloy.

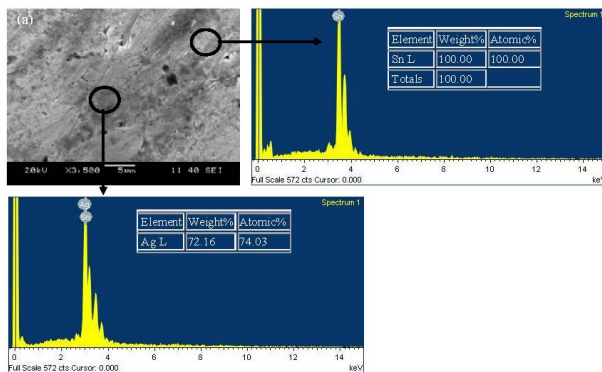


Fig. 9. (a) SEM of Sn–2Ag–0.7Cu; (b), (c) EDX analysis of the sample.

colored spots containing both Ag and Sn, approximately in the stoichiometric ratio 3:1 (Fig. 9c). These are possibly intermetallic Ag_3Sn . The formation of Ag_3Sn becomes even more prominent when the wt.% of Ag is increased to 2.5 wt.% in Sn–2.5Ag–0.7Cu alloy. The DSC analysis in Fig. 10 shows that the melting point of Sn–2Ag–0.7Cu alloy is 229.08 °C.

Sn–2.5Ag–0.7Cu alloy was developed by adding 2.5 wt.% of Ag and 0.7 wt.% Cu into molten Sn which was followed by stirring for few minutes. The melt was subsequently held at 700 °C for 2 h after which the alloy was cooled in the furnace to room temperature. Ag–Sn and Cu–Sn intermetallic compounds are found in the Sn–2Ag–0.7Cu solder alloy. The SEM as well as EDX analysis in Fig. 11a, 11b and Fig. 11c, respectively, show that the edge of the eutectic

region contains intermetallic Ag_3Sn . Intermetallic Ag_3Sn precipitates near the dark regions which are intermetallic Cu_6Sn_5 . The microstructural analysis confirms the presence of the fine Ag_3Sn particles dispersed in β -Sn matrix. The elemental mapping of Sn, Cu and Ag is shown in Fig. 11d, 11e and 11f, respectively. The interfacial bonding between these two phases results in excellent mechanical properties of this alloy. However, Ag_3Sn is brittle in nature which may degrade the reliability of the solder joint. The dark regions are the intermetallic Cu_6Sn_5 . Liquid Sn is known to provide a rapid diffusion medium for Ag and Cu. Thus, once intermetallic compounds, like Ag_3Sn or Cu_6Sn_5 have nucleated, pronounced growth of one or both of these intermetallic compounds takes place and relatively large precipitates can be observed in the microstructure [18].

The DSC plot in Fig. 12 shows that when the Ag wt.% is raised to 4.5 wt.% in Sn–4.5Ag–0.7Cu lead free solder alloy, the melting point comes down to 226.89 °C. Addition of higher amount of Ag gradually reduces the melting point of the eutectic Sn–0.7Cu solder alloy. The melting temperature of Sn–4.5Ag–0.7Cu solder alloy (226.89 °C) is lower than the melting point of the eutectic Sn–0.7Cu solder alloy, which is 234.89 °C.

Fig. 13a shows the variation of the melting point of the Sn–Cu solder alloy with addition of Ag. There is a gradual decrease in the melting temperature of the solder alloy as the wt.% of Ag is

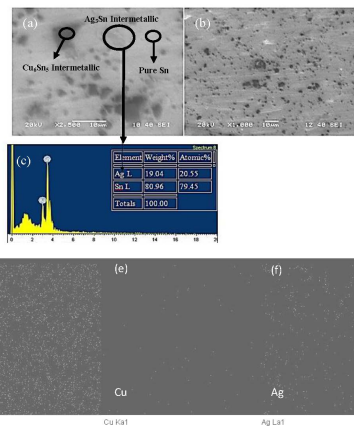


Fig. 11. (a), (b) SEM of Sn–2.5Ag–0.7Cu; (c) EDX analysis of the sample. Elemental mapping of (d) Sn (e) Cu and (f) Ag of the region shown in the SEM image in Fig. 11a.

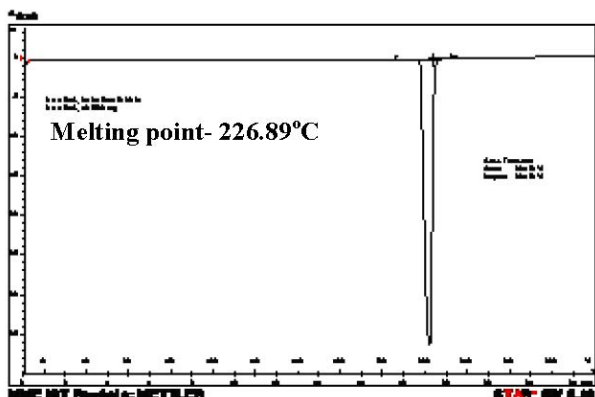


Fig. 12. DSC of Sn–4.5Ag–0.7Cu lead free solder alloy.

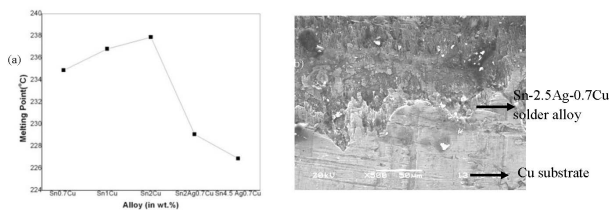


Fig. 13. (a) Variation of melting temperature of the Sn–Cu solder alloy with addition of Ag; (b) Microstructure of Sn–2.5Ag–0.7Cu solder alloy soldered to Cu substrate.

increased in the Sn–0.7Cu eutectic alloy. When the Cu wt.% is raised from 0.7 to 2 wt.%, the melting point increases. When the Ag wt.% increases in the eutectic Sn–0.7Cu alloy, the melting point

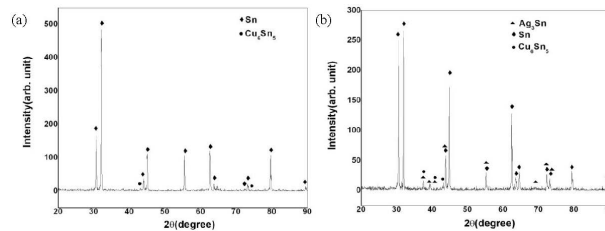


Fig. 14. X-ray diffraction plots of (a) Sn–0.7Cu and (b) Sn–2Ag–0.7Cu lead free solder alloys.

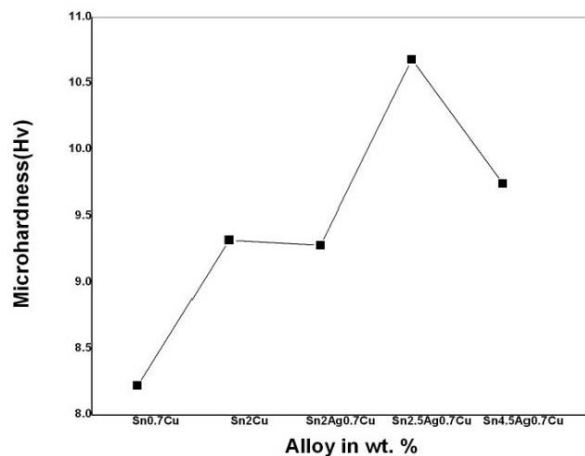


Fig. 15. Variation of hardness with increase in wt.% of Ag in Sn–0.7Cu eutectic composition.

decreases and goes below the melting point of the eutectic Sn–0.7Cu solder alloy. Ag is very effective in reducing the melting temperature of the eutectic Sn–0.7Cu solder alloy.

Fig. 13b shows the interface between the Sn–2.5Ag–0.7Cu solder alloy and the Cu substrate. Here, the Sn–2.5Ag–0.7Cu was used as a solder alloy on a Cu substrate. The SEM image shows good wettability and bonding between the Cu substrate and the Sn–2.5Ag–0.7Cu solder alloy.

The X-ray diffraction plots in Fig. 14a and 14b show that in both the alloys, Sn–0.7Cu and Sn–2Ag–0.7Cu, formation of intermetallic Cu_6Sn_5 takes place. Fig. 14b shows the formation of intermetallic phase Ag_3Sn in the case of Sn–2Ag–0.7Cu alloy, in addition to intermetallic compound Cu_6Sn_5 . The alloy containing high wt.% of Ag, like Sn–2Ag–0.7Cu, exhibits the formation of Ag_3Sn intermetallic compound.

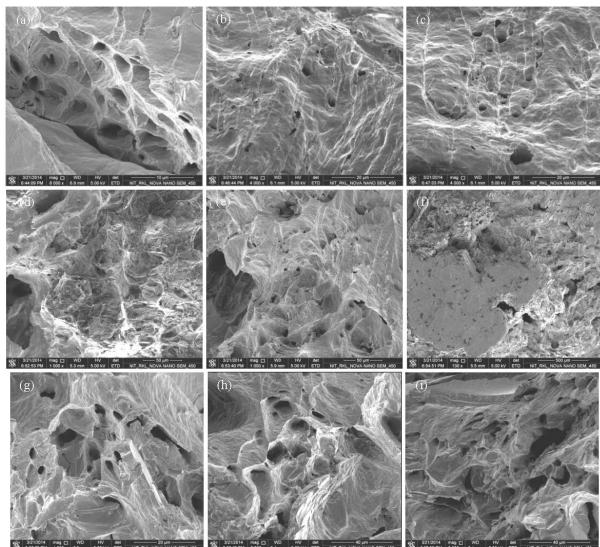


Fig. 16. SEM images of the fracture surfaces of (a), (b), (c) Sn-0.7Cu, (d), (e), (f) Sn-2Ag-0.7Cu, (g), (h), (i) Sn-4.5Ag-0.7Cu alloys.

The plot in Fig. 15 shows the variation of microhardness with increasing wt.% of Ag in the Sn-0.7Cu eutectic composition. It shows that the hardness of the Sn-0.7Cu eutectic composition increases initially with addition of Ag up to 2.5 wt.%. The increase in hardness of Sn-0.7Cu eutectic solder alloy due to the addition of Ag results possibly from the strengthening effect of Ag_3Sn phase. It appears that the presence of Ag_3Sn in Sn-Cu-Ag solder might act as potential sites for obstructing the localized deformation of the matrix during the motion of dislocations and grain boundaries. It should be noted that the hardness of the intermetallic phase Cu_6Sn_5 is greater than the hardness of intermetallic compound Ag_3Sn . So, the addition of higher wt.% of Ag to the Sn-0.7Cu solder alloy leads to the formation of Ag_3Sn which is softer compared to the Cu_6Sn_5 intermetallic compound and eventually reduces the hardness of the solder alloy. This is possibly the reason why on increasing the wt.% of Ag above 2.5 wt.% in the eutectic composition of Sn-0.7Cu, the hardness of the alloy decreases. The microstructural changes cause the decrease of hardness of the solder alloy [1, 19].

The fracture surface developed in various Sn-Ag-Cu solder alloys was also analyzed.

Fig. 16a – 16i show the SEM images of the fracture surface of the three Sn-0.7Cu, Sn-2Ag-0.7Cu and Sn-4.5Ag-0.7Cu solder alloys. The fractographs of Sn-0.7Cu solder alloy in Fig. 16a – 16c show a ductile nature of the fractures, confirmed by the formation of dimples. The fracture surfaces of Sn-2Ag-0.7Cu alloy in Fig. 16d and 16f show the brittle nature of the alloy fracture. The flat smooth fracture surface indicating the brittle fracture could be clearly seen in Fig. 16f. There is also absence of dimples in the fracture surface. The fracture surface of Sn-4.5Ag-0.7Cu alloy in Fig. 16g – 16i shows dimple formation on the fracture surface. This indicates that higher wt.% of Ag in the alloy leads to an increase in the ductile nature of the fracture. Lower wt.% of Ag in the alloys leads to brittle failure of the sample. The absence of Ag in Sn-0.7Cu alloy also results in ductile nature of the fracture of the sample [20–22].

The lead free solder alloys are predominantly Sn based alloys. So far, eutectic or near eutectic Sn-Pb alloys have been very widely used as solder material due to their low melting temperature (183 °C) and good wettability. Sn-Zn alloys are known to have good mechanical properties and their melting point (198 °C) is similar to that of Sn-Pb eutectic solder (183 °C). High mechanical integrity of electronic packaging, manufacturability and relatively low cost are some of the major advantages of this solder alloy. However, Sn-Zn alloys get easily oxidized and have relatively poor wettability. In order to improve the oxidation resistance and wettability, Ag is added to the Sn-8Zn near eutectic composition. The effects of addition of third element Ag on the microstructure and melting temperature of the near eutectic Sn-8Zn solder alloy was also investigated.

The Sn-Zn eutectic alloy has been considered as one of the potential lead-free solders that can replace the Sn-37Pb solder. The major drawbacks of this alloy are its poor wettability and oxidation. The phase diagram of the Sn-Zn binary system is given below in Fig. 17a. Fig. 17b and Fig. 17c show the binary phase diagram of Zn-Ag and Sn-Ag systems, respectively. Fig. 17d is the ternary phase diagram of Sn-Zn-Ag

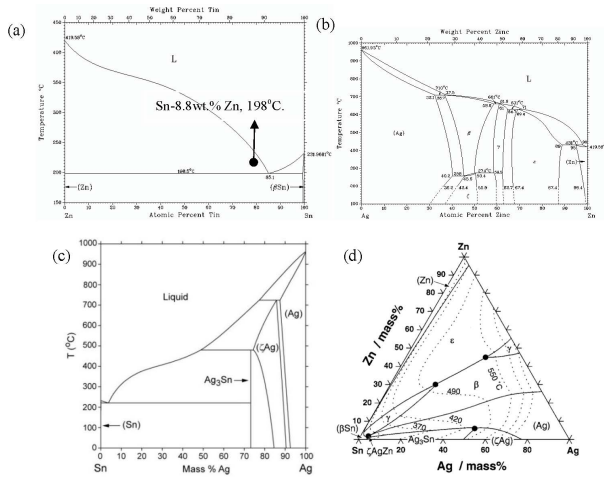


Fig. 17. (a) Sn–Zn, (b) Zn–Ag, (c) Sn–Ag phase diagram, (d) Sn–Zn–Ag ternary phase diagram [23].

system [23]. The ternary phase diagram of Sn–Zn–Ag system shows the presence of several intermetallics in the system. The Sn–8Zn, Sn–8Zn–0.05Ag, Sn–8Zn–0.1Ag, Sn–8Zn–0.2Ag (wt.%) solder alloys were developed.

Here, Ag has been added to the near eutectic Sn–8Zn solder alloy to study the effect of Ag on this composition. Fig. 18 shows the microstructure of the Sn–8Zn–0.05Ag, Sn–8Zn–0.1Ag and Sn–8Zn–0.2Ag solder alloys. The microstructural features are similar to the Sn–Zn eutectic microstructure. The microstructure consists mainly of proeutectic β -Sn phase, needle-like Zn-rich phase and Ag–Zn intermetallics. The microstructure of the Sn–8Zn–0.05Ag solder alloy consists of a large primary β -Sn phase. With the increase in the content of Ag, the Ag–Zn intermetallic phase increases as in the Sn–8Zn–0.2Ag alloy (Fig. 18h – 18j). Peaks of AgZn_3 could be seen in the X-ray diffraction plot of Sn–8Zn–0.2Ag solder alloy (Fig. 23). AgZn_3 nodular intermetallic phase precipitation takes place and these intermetallics deplete the Zn-rich phase. The growth of the AgZn_3 intermetallic compound is accelerated by increasing the wt.% of Ag in the solder alloy [24, 25].

Fig. 19 shows the SEM image of Sn–8Zn–0.05Ag solder alloy along with the elemental maps of Sn, Zn and Ag. The microstructure

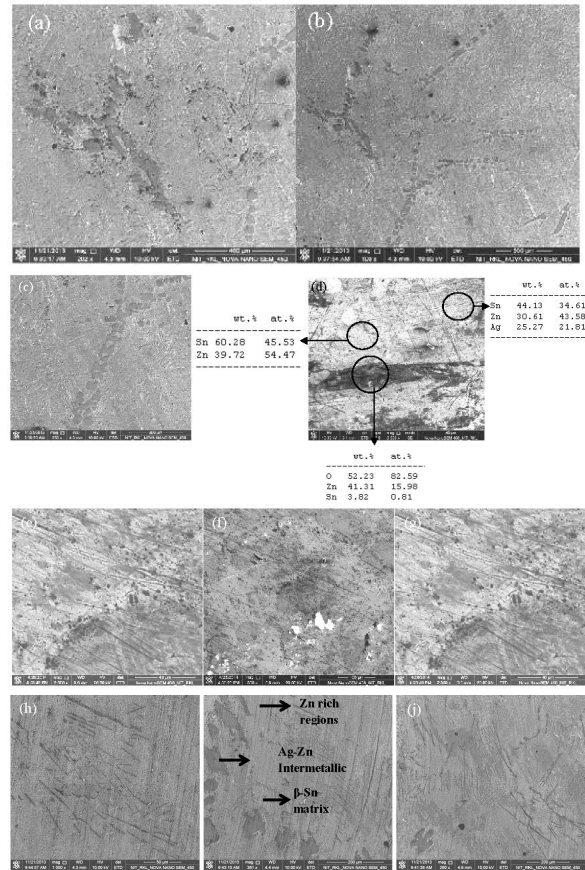


Fig. 18. SEM images of (a), (b), (c), (d) Sn–8Zn–0.05Ag, (e), (f), (g) Sn–8Zn–0.1Ag, (h), (i), (j) Sn–8Zn–0.2Ag.

consists of Sn, Sn/Zn eutectic, needle-like precipitate of the Zn-rich phase and Ag–Zn intermetallic compound. In the SEM micrograph, the light regions represent the Sn rich matrix, while the dark regions represent the Ag–Zn intermetallic compound. It is very clear from the elemental maps that the dark colored Zn-rich regions are surrounded by the Sn rich matrix consisting mainly of Sn. Needle-like Zn-rich phase could be seen in the microstructure. Zn is present only in the dark colored regions and these regions contain no Sn at all.

It should be noted that the mutual solubility of Sn and Zn at room temperature is almost nil (Fig. 17a). Sn–Zn binary phase diagram shows very low solubility of Zn in solid Sn, and the Ag–Zn system phase diagram in Fig. 17b shows

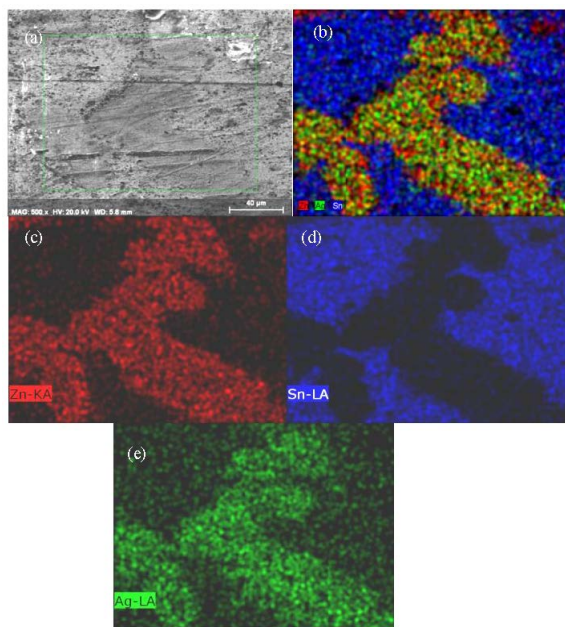


Fig. 19. (a) FESEM image of Sn-8Zn-0.05Ag solder alloy (b) combined elemental mapping of Sn, Zn and Ag and elemental mapping of (c) Zn, (d) Sn, (e) Ag.

that large amounts of Zn are readily soluble in solid Ag. Sn is present in the light colored matrix region only. Ag is also present in the region containing Zn. This suggests the formation of intermetallic Ag-Zn compound in this region. The amount of the Ag-Zn intermetallic compounds increased with increasing Ag content in the alloy, thus, depleting the Zn-rich phase in the alloy containing high Ag content. X-ray diffraction pattern in Fig. 23 also shows the formation of AgZn_3 intermetallic compound in the Sn-8Zn-0.1Ag and Sn-8Zn-0.2Ag compositions. An increase in the quantity of intermetallic Ag-Zn compound could lower the ductility of the solder alloy as intermetallic compounds are known to be brittle in nature. Fig. 19, Fig. 20 and Fig. 21 show the elemental mapping of Zn, Sn and Ag in Sn-8Zn-0.05Ag, Sn-8Zn-0.1Ag and Sn-8Zn-0.2Ag solder alloys, respectively. The intermetallic phase AgZn_3 forms dendrites upon cooling as is evident from the SEM images in Fig. 18 and the elemental maps of Ag and Zn in Fig. 19 – 21.

Although it is clear from the binary Sn-Ag phase diagram in Fig. 17b and the ternary phase diagram in Fig. 17d that although intermetallic compounds of Ag, such as the $\epsilon\text{-AgZn}_3$, $\gamma\text{-Ag}_5\text{Zn}_8$ and Ag_3Sn , are possible in this system but Ag forms only intermetallic compound AgZn_3 with Zn. This is due to the lower enthalpy of formation of Ag-Zn intermetallic compounds, like $\epsilon\text{-AgZn}_3$ and $\gamma\text{-Ag}_5\text{Zn}_8$, compared to the enthalpy of formation of Ag_3Sn .

The DSC plot in Fig. 22a shows an endothermic peak at 210.1 °C. This is the melting point of the Sn-8Zn near eutectic alloy. The DSC plot in Fig. 22b shows a single sharp endothermic peak at 215.48 °C. This corresponds to the melting point of Sn-8Zn-0.05Ag. The melting point of the Sn-8Zn-0.05Ag solder alloy is slightly higher than the melting point of the near eutectic Sn-8Zn solder alloy. The DSC of Sn-Zn-0.1Ag solder alloy in Fig. 22c shows that the melting point of the alloy is 198.7 °C. Thus, there is a reduction in

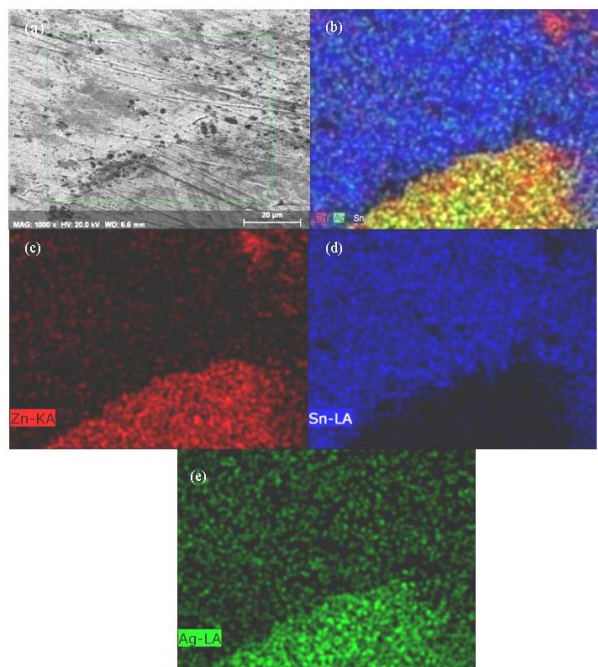


Fig. 20. (a) FESEM image of Sn-8Zn-0.1Ag solder alloy, (b) combined elemental mapping of Sn, Zn and Ag and elemental mapping of (c) Zn, (d) Sn, (e) Ag.

the melting point of the eutectic composition after addition of 0.1 wt.% Ag to Sn–8Zn near eutectic alloy but instead of a single sharp peak we can see two peaks in the DSC plot. This is due to the addition of Ag. The liquidus line of the Sn–Zn eutectic alloy rises with the increase of the Ag content in the alloy. This leads to an increase in the pasty region. It can be noted that the height of the first peak in the DSC plots decreases with an increase in the Ag content in the alloy. The small shoulder peak is observed at around 220 °C in the DSC curves for Sn–8Zn–0.1Ag and Sn–8Zn–0.2Ag alloys (Fig. 22c, 22d). This shoulder peak is not present in Sn–8Zn–0.05Ag solder alloy. The addition of a large amount of Ag into the Sn–8Zn–0.1Ag and Sn–8Zn–0.2Ag alloys resulted in the formation of larger amount of AgZn_3 intermetallic compound. This reaction reduced the Zn content of the near eutectic Sn–8Zn composition which caused the formation of a hypoeutectic β -Sn structure. This is why the DSC plots of the Sn–8Zn–0.1Ag and Sn–8Zn–0.2Ag solder alloys

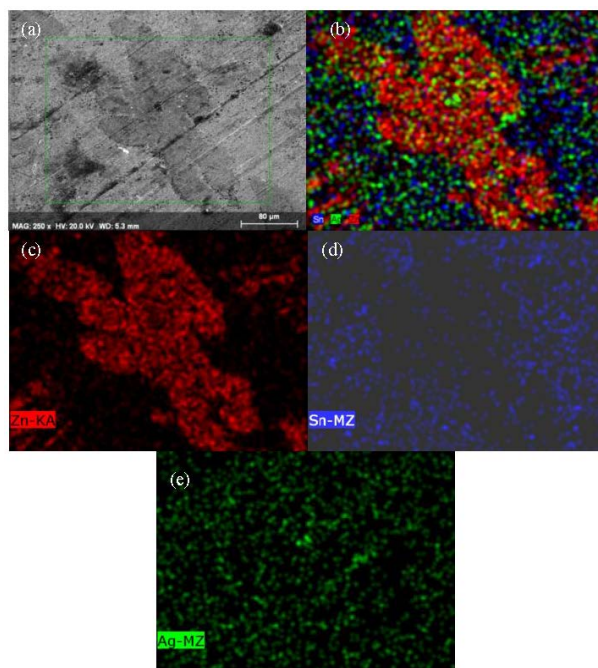


Fig. 21. (a) FESEM image of Sn–8Zn–0.2Ag solder alloy, (b) combined elemental mapping of Zn, Sn and Ag and elemental mapping of (c) Zn, (d) Sn, (e) Ag.

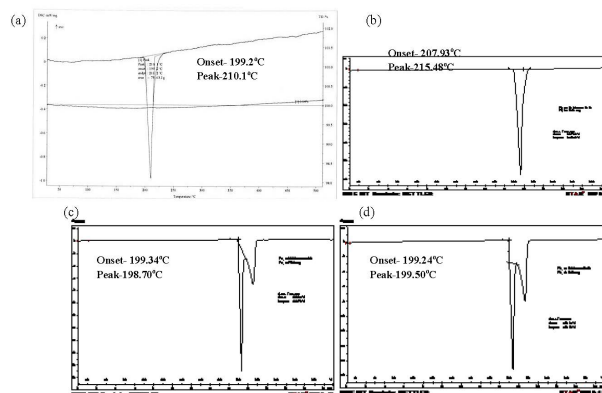


Fig. 22. DSC of (a) Sn–8Zn (near eutectic), (b) Sn–Zn–0.05Ag, (c) Sn–Zn–0.1Ag, (d) Sn–Zn–0.2Ag solder alloy.

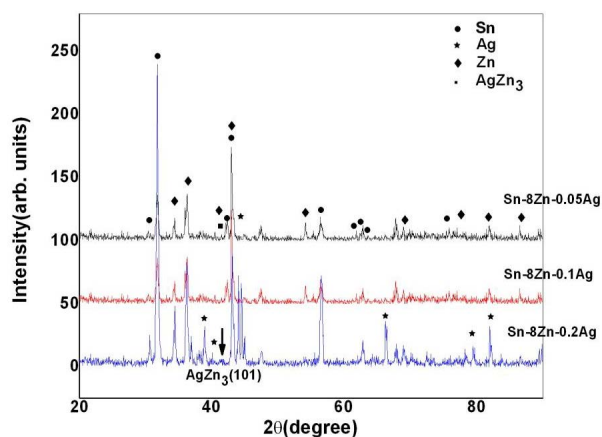


Fig. 23. X-ray diffraction plots of Sn–8Zn–0.05Ag, Sn–8Zn–0.1Ag and Sn–8Zn–0.2Ag solder alloys.

show two endothermic peaks. The first endothermic peak represents the melting of the eutectic Sn–Zn–Ag ternary system and the other peak is due to the melting of the hypoeutectic β -Sn [26–28].

The X-ray diffraction analysis in Fig. 23 suggests that there is a possibility of formation of intermetallic AgZn_3 in Sn–8Zn–0.1Ag and Sn–8Zn–0.2Ag compositions. The X-ray diffraction plot of Sn–8Zn–0.2Ag shows a small peak having low intensity, corresponding to that of AgZn_3 (101). The intensity of this peak is low due to the low volume fraction of the formed intermetallic compound as Ag content in the alloy is only 0.2 wt.%. The AgZn_3 (101) peak has

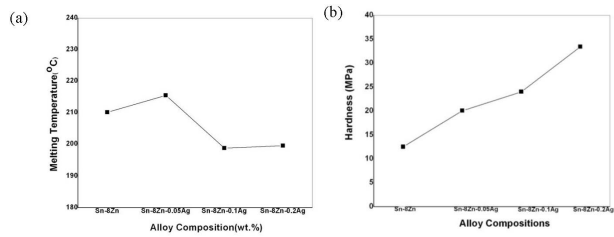


Fig. 24. Variation of (a) melting point (b) hardness of the various Sn–Zn–Ag solder alloys with addition of Ag.

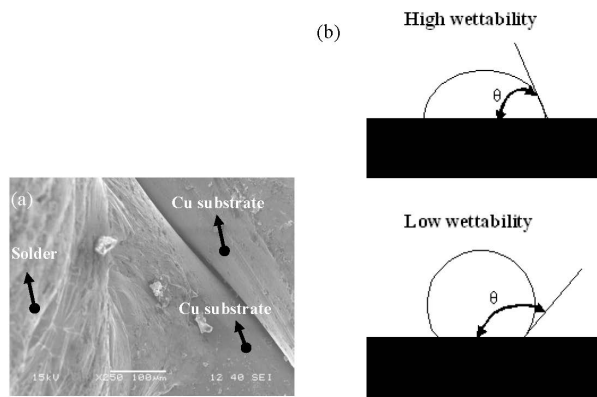


Fig. 25. (a) SEM of the contact between the Sn–8Zn near eutectic solder and Cu substrate (b) Schematic showing the contact angle (θ) between a liquid and a substrate.

been marked using an arrow. The AgZn_3 intermetallic phase depletes the Zn-rich phase and is present in the form of inhomogeneous dendrites. The growth of Ag_3Zn nodular compounds is accelerated by the higher wt.% of Ag in the alloy. The result of XRD analysis clearly shows that the Sn–Zn–Ag solder alloy forms the AgZn_3 intermetallic compound when the content of Ag is higher than 0.2 wt.% but the intermetallic compound AgZn_3 was not detected when the Ag content was lower than 0.2 wt.% [29, 30].

Fig. 24a shows the variation of melting point with addition of Ag to the Sn–8Zn near eutectic solder alloy. It should be noted that addition of 0.05 wt.% of Ag slightly increases the melting temperature of the near eutectic Sn–8Zn solder alloy, whereas adding 0.1 wt.% Ag reduces the melting temperature to a great extent. Further addition of Ag (0.2 wt.%) leads to a slight increase

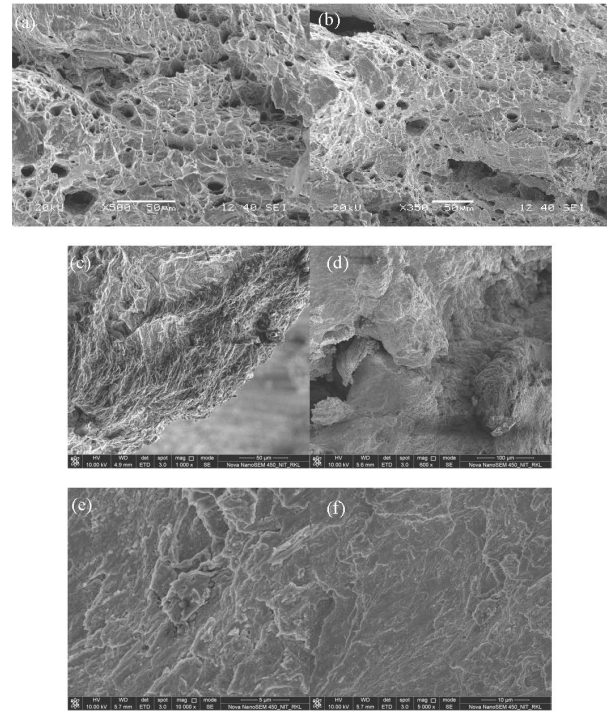


Fig. 26. SEM image showing the fracture surface of (a), (b) Sn–8Zn, (c), (d) Sn–8Zn–0.1Ag (e), (f) Sn–8Zn–0.2Ag solder alloys.

in the melting point of the eutectic composition to 199.5 °C. Thus, it is possible to reduce the melting point of the Sn–8Zn near eutectic alloy by adding low wt.% of Ag. The addition of Ag between 0.05 and 0.1 wt.% to the Sn–8Zn near eutectic composition leads to a decrease in the melting point. Fig. 24b shows the variation of hardness of various Sn–Zn–Ag solder alloys with addition of Ag. The Sn–8Zn near eutectic alloy shows a gradual rise in the hardness with addition of Ag. Ag additions to the Sn–8Zn near eutectic alloy led to the formation of Ag–Zn intermetallic compound, AgZn_3 , and possibly this has led to higher hardness of the Sn–8Zn solder alloys upon addition of Ag. Low Ag content up to 0.2 wt.% to the near eutectic Sn–8Zn solder alloy led to the formation of large amounts of uniformly distributed fine Zn-rich needle-like structures which gave rise to dispersion strengthening effect and this also led to increase in hardness [31].

The Sn–8Zn near eutectic solder alloy has been used for Cu wires. Fig. 25a shows the SEM

image of the region of contact between the solder and the Cu wire. The contact angle (θ) of a liquid with a solid is used as a wettability measure. When $\theta < 90^\circ$ it is assumed that the liquid wets the substrate, whereas for $\theta > 90^\circ$ the liquid does not wet the substrate (Fig. 25b). When $\theta = 0^\circ$, the liquid completely wets the substrate. The Sn–8Zn near eutectic solder alloy shows very good wettability of the Cu wire. The angle of wetting (θ) between the solder alloy and the Cu substrate, which is a measure of the wettability of a liquid on a surface, is very low and this suggests that there is very good wetting between the alloy and the Cu substrate.

Fig. 26 shows the SEM images of the fracture surface of Sn–8Zn, Sn–8Zn–0.1Ag and Sn–8Zn–0.2Ag solder alloys. The fracture surfaces of all the alloys show the presence of ductile dimples, indicating ductile fracture. A typical ductile mode of fracture could be seen in the case of Sn–Zn–Ag solder having low wt.% of Ag. On the other hand, as the wt.% of Ag in the Sn–Zn–Ag solder alloy increases, a mixed ductile and brittle fracture could be observed. As Ag combines with Zn to form an Ag–Zn intermetallic compound, stress concentration can occur at the interface between the intermetallic Ag–Zn compound and the matrix phase and this can give rise to a more brittle fracture [30–33].

4. Conclusions

In the present work, the effect of addition of Ag to Sn–0.7Cu eutectic and Sn–8.8Zn near eutectic alloys on the microstructure and formation of intermetallic compounds was investigated. Mechanical properties, like hardness and fracture mode of various Sn–Ag–Cu and Sn–Zn–Ag solder alloys, were also investigated. The results are summarized as follows:

1. A reduction in melting point was observed upon addition of Ag to the eutectic Sn–0.7Cu solder alloy. The melting point of the eutectic Sn–0.7Cu alloy was found to be 234.88°C and it decreased to 226.89°C upon alloying with 4.5 wt.% Ag in Sn–4.5Ag–0.7Cu solder alloy.
2. The hardness of the Sn–0.7Cu eutectic composition increased with addition of Ag up to 2.5 wt.%, whereas upon increasing the wt.% of Ag above 2.5 wt.% in the eutectic composition of Sn–0.7Cu, the hardness of the alloy decreased.
3. Addition of Ag to Sn–Ag–Cu solder alloys led to the formation of intermetallic compound Ag_3Sn . Cu_6Sn_5 was found in both Sn–Cu as well as in Sn–Ag–Cu solder alloys.
4. Addition of lower wt.% of Ag (2 wt.%) to the Sn–0.7Cu eutectic alloy led to a brittle fracture of the alloy. When the wt.% of Ag in the alloy was increased, the nature of fracture was found to be ductile. The absence of Ag in the Sn–0.7Cu eutectic alloy resulted in ductile nature of failure.
5. Addition of up to 0.1 wt.% Ag to Sn–8Zn near eutectic composition led to a reduction in melting point but further addition of Ag (0.2 wt.%) led to slight rise in the melting point.
6. A shoulder was observed at around 220°C in the DSC curves of Sn–8Zn–0.1Ag and Sn–8Zn–0.2Ag alloys. This shoulder was not present in 0.05 wt.% Ag containing solders. The addition of a large amount of Ag into the Sn–8Zn–0.1Ag and Sn–8Zn–0.2Ag alloys resulted in the formation of large amount of AgZn_3 intermetallic compound. This reaction reduced the Zn content in the eutectic Sn–Zn composition which resulted in the formation of a hypoeutectic β -Sn structure. This is why the DSC plots of the solder alloys Sn–8Zn–0.1Ag and Sn–8Zn–0.2Ag showed two endothermic peaks.

Acknowledgements

We would like to thank the staff of the thermal analysis, FESEM, SEM and XRD laboratories at the National Institute of Technology Rourkela, India. We would also like to thank everyone involved at the National Institute of Technology Rourkela for their useful feedback and help.

References

- [1] EL-DALY A.A., HAMMAD A.E., *J. Alloy. Compd.*, 509 (34) (2011), 8554.
- [2] WU C.M.L., HUANG M.L., *J. Electron. Mater.*, 31 (5) (2002), 442.
- [3] REDDY B., BHATTACHARYA P., SINGH B., CHATTOPADHAYA K., *J. Mater. Sci.*, 44 (2009), 2257.
- [4] EL-DALY A.A., EL-TAHER A.M., DALLOUL T.R., *Mater. Design*, 55 (2014), 309.
- [5] ROSALBINO F., ANGELINI E., ZANICCHI G., MARAZZA R., *Mater. Chem. Phys.*, 109 (2008), 386.
- [6] KANG S.K., SHIH D.Y., LEONARD D., HENDERSON D.W., GOSSELIN T.C., SUNG-IL YU J., CHOI W.K., *JOM*, 56 (6) (2004), 34.
- [7] EL-DALY A.A., HAMMAD A.E., *Mater. Design*, 40 (2012), 292.
- [8] ZHANG L., BAIXUE S., GAO L., CHEN Y., YU S., SHENG Z., ZENG G., *J. Mater. Sci.- Mater. El.*, 20 (2009), 1193.
- [9] YU D.Q., ZHAO J., WANG L., *J. Alloy. Compd.*, 376 (1 – 2) (2004), 170.
- [10] MUDRYI S.I., SHATBLAVYI I.I., SKLYARCHUK V.I., PLEVACHUK Y.O., KOROLYSHYN A.V., YAKYMOVYCH A.S., *Mater. Sci.*, 46 (4) (2011), 464.
- [11] BIOCCA P., *Creating Solder Joint Reliability with SnCu Based Solders Some Practical Experiences*, Kester, Illinois, USA, 2009.
- [12] MILLER C.M., ANDERSON I.E., SMITH J.F., *J. Electron. Mater.*, 23 (7) (1994), 595.
- [13] OHNUMA I., MIYASHITA M., ANZAI K., LIU X.J., OHTANI H., KAINUMA R., ISHIDA K., *J. Electron. Mater.*, 29 (10) (2000), 1137.
- [14] KINNEY C., LINARES X., LEEK O., MORRIS J.W., *J. Electron. Mater.*, 42 (4) (2013), 607.
- [15] KIM K.S., HUH S.H., SUGANUMA K., *J. Alloy. Compd.*, 352 (1 – 2) (2003), 226.
- [16] KARAKAYA I., THOMPSON W.T., *Bull. Alloy Phase Diagr.*, 8 (4) (1987), 340.
- [17] SUBRANMANIAN P.R., PEREPEZKO J.H., *J. Phase Equilib. Diff.*, 14 (1) (1993), 62.
- [18] LEHMAN L.P., ATHAVALE S.N., FULLEM T.Z., GIAMIS A.C., KINYANJUI R.K., LOWENSTEIN M., MATHER K., PATEL R., RAE D., WANG J., XING Y., ZAVALI L., BORGESSEN P., COTTS E.J., *J. Electron. Mater.*, 33 (12) (2004), 1429.
- [19] EL-DALY A.A., EL-TANTAWY F., HAMMAD A.E., GAAFAR M.S., EL-MOSSALAMY E.H., AL-GHAMDI A.A., *J. Alloy. Compd.*, 509 (26) (2011), 7238.
- [20] FREITAS E.S., OSORIO W.R., SPINELLI J.E., GARCIA A., *Microelectron. Reliab.*, 54 (6 – 7) (2014), 1392.
- [21] YOU T., KIM Y., JUNG W., MOON J., CHOE H., *J. Alloy. Compd.*, 486 (1 – 2) (2009), 242.
- [22] HU X., CHEN W., WU B., *Mat. Sci. Eng. A-Struct.*, 556 (2012), 816.
- [23] OHNUMA I., LIU X.J., OHTANI H., ISHIDA K., *J. Electron. Mater.*, 28 (11) (1999), 1164.
- [24] LUO T., CHEN Z., HU A., LI M., *Mat. Sci. Eng. A-Struct.*, 556 (2012), 885.
- [25] WEI C., LIU Y.C., HAN Y.J., WAN J.B., YANG K., *J. Alloy. Compd.*, 464 (1 – 2) (2008), 301.
- [26] SONG J.M., LIN K.L., *J. Mater. Res.*, 18 (9) (2003), 2060.
- [27] CHEN K.I., LIN K.L., *J. Electron. Mater.*, 31 (8) (2002), 861.
- [28] AHMED M., FOUZDER T., SHARIF A., GAIN A.K., CHAN Y.C., *Microelectron. Reliab.*, 50 (2010), 1134.
- [29] LIN K.L., SHIH C.L., *J. Electron. Mater.*, 32 (12) (2003), 1496.
- [30] CHEN K.I., CHENG S.C., WU S., LIN K.L., *J. Alloy. Compd.*, 416 (2006), 98.
- [31] SONG J.M., LAN G.F., LUI T.S., CHEN L.H., *Scripta Mater.*, 48 (8) (2003), 1047.
- [32] SONG J.M., LUI T.S., LANG F., CHEN L.H., *J. Alloy. Compd.*, 379 (1 – 2) (2004), 233.
- [33] LUO T., CHEN Z., HU A., LI M., LI P., *Microelectron. Reliab.*, 53 (12) (2013), 2018.

Received 2014-08-14

Accepted 2015-02-11